THE ASTROPHYSICAL JOURNAL, 340:181–189, 1989 May 1

BULK ACCELERATION IN RELATIVISTIC JETS AND THE SPECTRAL PROPERTIES OF BLAZARS

GABRIELE GHISELLINI
Institute of Astronomy, Cambridge

AND

LAURA MARASCHI
Dipartimento di Fisica, Universita' di Milano
Received 1988 June 7; accepted 1988 September 22

ABSTRACT

Models for the synchrotron and inverse Compton emission from relativistic jets with bulk acceleration are studied. The basic scheme explored is that the bulk velocity increases with increasing distance along the jet, while the emission spectrum shifts to lower frequencies. Thus synchrotron X-rays, emitted by the jet core, are weakly beamed, while the optical and radio emissions, produced further away, are more strongly beamed. We find that the different broad-band spectra of BL Lac objects selected by radio or X-ray flux can be accounted for as due to different orientation, radio-selected objects being viewed at small angles, X-ray–selected objects at large angles. Stringent conditions are imposed by this requirement on the jet properties. In particular, acceleration should occur slowly over a wide distance range, with small final bulk Lorentz factors $\Gamma \simeq 3$–5. The space density of X-ray–selected BL Lac objects is expected to be 20–100 times that of radio selected BL Lac objects with the same X-ray luminosity. Synchrotron emission with steep spectrum is expected to be the main radiation mechanism in the X-ray band for objects seen at large angles. Inverse Compton emission, yielding flatter spectra and longer variability time scales, may be important in the X-ray band, especially for objects seen at small angles.

Subject headings: BL Lacertae objects — galaxies: jets — galaxies: nuclei — radiation mechanisms

I. INTRODUCTION

The presence of relativistic bulk motion in the cores of compact radio sources seems well established on the basis of the observational evidence (e.g., Blandford 1987). This leads to the necessary consequence that the emission is beamed in the direction of motion and the observed properties depend on the angle of the line of sight to the bulk velocity.

BL Lac objects are a special class of compact radio sources exhibiting a continuum which extends to the optical and up to the X-ray band. They are characterized by high polarization, rapid variability, and by the weakness of emission lines. Blandford and Rees (1978) first proposed that relativistic beaming would resolve the difficulties associated with the rapid variability and the strength of the nonthermal continuum in BL Lac objects, and since then this idea has gained wide support.

Models of emission from relativistic jets (Marscher 1980; Königl 1981; Reynolds 1982) reproduce the observed energy distribution by a convolution of spectra produced locally in different regions of the jet. In particular, since variability time scales are generally shorter at higher frequencies (Maraschi 1987; Impey and Neugebauer 1988), X-rays should be produced in the most compact region of the jet, i.e., nearest to the core (Ghisellini, Maraschi, and Treves 1985, hereafter Paper I). Recently, it has been suggested by various authors (Stocke *et al.* 1984; Maraschi *et al.* 1986, Browne and Murphy 1987) that the X-ray emission of BL Lac objects is more isotropic than their radio emission. This may be understood assuming that the bulk velocity of the plasma increases with increasing distance from the core (i.e., that the flow undergoes bulk acceleration), while the characteristic emission shifts to lower frequencies.

In the above scheme lower frequencies are increasingly boosted with respect to X-rays. Therefore the observed spectrum will depend on the viewing angle, being steeper for smaller angles. This qualitative prediction agrees with the finding that the overall spectra of BL Lac objects selected by different techniques differ significantly; radio selection, which, in the beaming hypothesis, favors small angles of view, yields steep overall spectra, while X-ray selection, which according to this scenario should be unbiased or less biased toward small angles, yields flatter overall spectra (Ghisellini *et al.* 1986; Maraschi *et al.* 1986).

In this paper we develop a quantitative model, following closely the approach of Paper I, but adding the consideration of a relativistic bulk velocity which increases with increasing distance. Our aim is to account for the average spectral shapes of the two groups of BL Lac objects (radio-selected and X-ray–selected) in terms of a single phenomenon viewed from different aspect angles. Within this model the average angles and bulk Lorentz factors can be derived, with important consequences on the inferred space densities and on the related problem of the "parent population." In fact, if this scenario is correct, objects in which the jet is at large angles to the line of sight, although weak at radio and optical frequencies, should be significant X-ray emitters.

Previous work regarding bulk acceleration in astrophysical jets has been done by Marscher (1980) and Reynolds (1982). Marscher (1980) treats the simplest case of an adiabatic accelerating jet and indeed finds that the observed spectrum is steeper when the jet is observed at small angles. Reynolds (1982) introduces an advanced treatment of hydrodynamic acceleration but neglects to consider explicitly the dependence of the observed spectra on viewing angle.

In § II we give a detailed account of the adopted jet model and approximate expressions for the observed synchrotron and inverse Compton spectra valid in limited spectral ranges. In § III we apply the model to the observed spectra of blazars. In § IV a general discussion of the results is given.

II. BASIC ASSUMPTIONS AND FORMULAE

A physical model for the jet is beyond the scope of this paper; therefore we will parametrize all functional dependences of the physical quantities along the jet axis with power laws and assume every quantity constant on surfaces normal to the jet axis. The shape of the jet is described by the dependence of the radius, r, of a cross section on the distance, R, from the central engine

$$r = r_0\left(\frac{R}{R_0}\right)^{\epsilon} \equiv r_0 x^{\epsilon} , \tag{1}$$

where R_0 and R_0 are the initial values. The ϵ parameter defines the geometry of the jet, $\epsilon = 1$ corresponding to a truncated cone, and $\epsilon < 1$ to a paraboloid. Hydrodynamic considerations (Blandford and Rees 1978; Reynolds 1982) show that in the region, $R < R_1$, where the flow undergoes bulk acceleration $\epsilon < 1$ and in the region after the terminal velocity is reached $\epsilon \simeq 1$.

For simplicity, the relativistic electron distribution $N(\gamma)$ is assumed to be a unique power law: $N(\gamma) = K\gamma^{-p}$ with the same slope p throughout the source, between $\gamma = 1$ and a maximum value $\gamma_{\max}$ which is allowed to vary with x as well as the density parameter K and the magnetic field B. We therefore have

$$\gamma_{\max} = \gamma_{\max}(R_0)x^{-\epsilon e} ; \tag{2}$$

$$K = K_0 x^{-\epsilon n} ; \tag{3a}$$

$$\tau \equiv \sigma_{\rm T} r K = \tau_0 x^{-\epsilon(n-1)} ; \tag{3b}$$

$$B = B_0 x^{-\epsilon m} . \tag{4}$$

In equation (3a) $\sigma_{\rm T}$ is the Thomson cross section. Consequently the local synchrotron spectrum is a power law of index $\alpha_0 = (p-1)/2$ up to a maximum synchrotron frequency

$$\nu_{\max} = \nu_{\max}(R_0)x^{-\eta} , \tag{5}$$

where $\eta = \epsilon(2e + m)$. In our model η is assumed to be positive, corresponding to the largest frequencies being produced at the base of the jet (see, e.g., Königl 1981 for a different choice).

The variation of the bulk Lorentz factor Γ with R is also described by a power law

$$\Gamma = x^{g} . \tag{6}$$

Because of the radial dependences of the magnetic field and of the particle density, the self-absorption frequency ν_m is a function of position

$$\nu_m = \nu_m(R_0)x^{-k_m} , \tag{7}$$

where $k_m = 2\epsilon[n + m(1.5 + \alpha_0) - 1]/(5 + 2\alpha_0)$ (see, e.g., Paper I).

The synchrotron emissivity $\epsilon_s(\nu, x)$ between the self-absorption frequency ν_m and the maximum synchrotron frequency $\nu_{\max}$ is given by

$$\epsilon_s(\nu, x) = \frac{c_1(\alpha_0)}{4\pi} K_0 B_0^{1+\alpha_0} x^{-n-m(1+\alpha_0)} \nu^{-\alpha_0} , \tag{8}$$

where $c_1(\alpha_0)$ takes the value 3.6×10^{-19} for $\alpha_0 = 0.5$ (see, e.g., Blumenthal and Gould 1970).

The observed synchrotron luminosity from a cross section of the jet of thickness $dx = (dR/R_0)$ is given by

$$dL_s(\nu) = 4\pi^2 \epsilon_s(\nu, x) R_0^3 x^{2\epsilon}[\delta(x, \theta)]^{2+\alpha} dx , \tag{9}$$

where $\delta(x, \theta)$ is the usual Doppler factor

$$\delta = \{\Gamma(x) - [\Gamma^2(x) - 1]^{1/2} \cos\theta\}^{-1} . \tag{10}$$

The dependence of $dL_s(\nu)$ on x, apart from the Doppler factor, can be summarized with an index ξ which incorporates the dependences of the magnetic field B and the relativistic particle density K on R so that

$$dL_s(\nu) = 4\pi^2 \epsilon_s(\nu, 1) R_0^3 x^{\xi-1}[\delta(x, \theta)]^{2+\alpha} dx , \tag{11}$$

where

$$\xi - 1 = \epsilon[2 - n - m(1 + \alpha_0)] . \tag{12}$$

For constant δ-factor (i.e., without acceleration), the sign of ξ determines whether most of the observed flux is produced in the inner ($\xi < 0$) or outer ($\xi > 0$) part of the jet.

The synchrotron spectrum from the whole jet is obtained by integration

$$L_s(\nu) = \int_{x_1(\nu)}^{x_2(\nu)} dL_s(\nu)$$
$$= 4\pi^2 R_0^3 \epsilon_s(\nu, 1)\nu^{-\alpha_0} \int_{x_1(\nu)}^{x_2(\nu)} x^{\xi-1}[\delta(x, \theta)]^{2+\alpha_0} dx . \tag{13}$$

Since the emission below the synchrotron self-absorption frequency ν_m can be neglected, the lower limit $x_1(\nu)$ is the largest between 1 and the distance at which $\delta(x_1)\nu_m(x_1) = \nu$. Analogously $x_2(\nu)$ is the minimum between the maximum extension of the jet, $x_{\max}$, and the distance at which the maximum synchrotron frequency $\delta(x_2)\nu_{\max}(x_2) = \nu$.

The self-Compton (hereafter IC) luminosity can be found in a way that is analogous to the synchrotron luminosity. We adopt here the simplifying assumption that the locally produced photons dominate the radiation energy density (local approximation). This assumption is discussed in Paper I, where it is shown to be a sufficient approximation for all cases of interest here. We also refer to Paper I for the relevant formulae, from which the specific luminosity $L_c(\nu)$ due to the Compton process can be derived

$$L_c(\nu) = \frac{3}{8} A(\alpha_0)\tau_0 K_0 B_0^{1+\alpha_0} R_0^3 \nu^{-\alpha_0}$$
$$\times \int_{x_1(\nu)}^{x_2(\nu)} x^{l-1}[\delta(x, \theta)]^{2+\alpha_0} \ln\left[\frac{\nu_2(R)}{\nu_1(R)}\right] dx . \tag{14}$$

The factor $A(\alpha_0)$ is listed in Paper I [$A(0.5) \sim 1.4$], ν_1, ν_2 are the extreme frequencies of the synchrotron spectrum contributing at a given inverse Compton frequency ν. For the cases of interest here, they can be approximated by $\nu_2(R) = \nu_{\max}(R)$ and $\nu_1(R) = \nu_m(R)$.

The parameter $l = \xi + \epsilon(1 - n)$ has for the Ic emission same role as ξ for the synchrotron one: $l > 0$ means that the outer regions of the jet are mostly contributing at the frequency ν, if $\delta(x)$ is constant. For the general case, the limits of integration are complicated and can be found, e.g., in Paper I. For the cases of interest here and for frequencies in the X-ray range, they coincide with the minimum and maximum size of the jet.

To illustrate the effects of the gradients of the physical parameters on the resulting spectra, let us consider the case of $\alpha_0 = 0.5$, $m = 1$ and $n = 2$. $\alpha = 0.5$ corresponds to $p = 2$ which

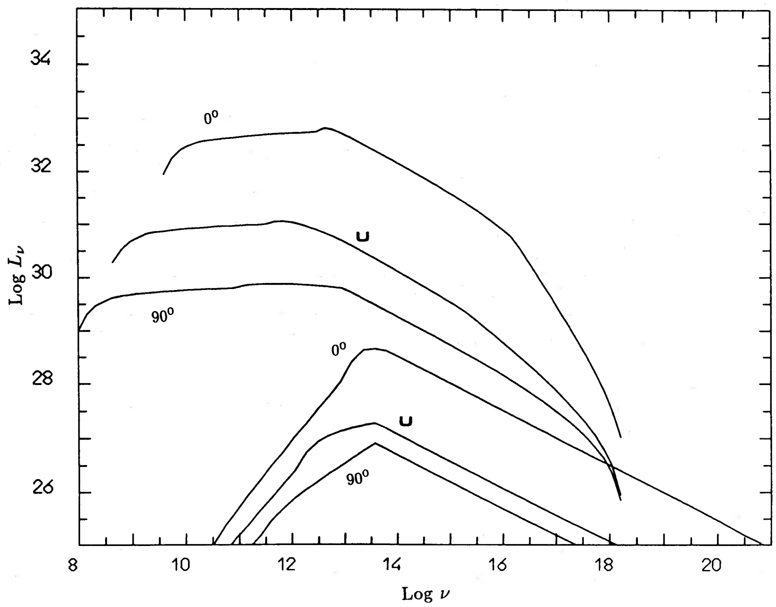

FIG. 1.—The synchrotron (*upper three tracings*) and inverse Compton (*lower three tracings*) emission spectra from a relativistic jet, described by the parameters reported in Table 1. The curve referring to the intrinsic (unbeamed) emission ($g = 0$ in Table 1) is labeled "*u*". The other curves represent the observed spectra for different angles of view when bulk acceleration is introduced in the inner region of the jet ($g = 0.2$ in Table 1).

is the equilibrium solution of the particle spectrum for continuous injection of high-energy particles (see, e.g., Kardashev 1962); $m = 1$, $n = 2$ correspond to a constant ratio of magnetic to particle energy density throughout the source. We further choose $\nu_{\max}(1) = 2 \times 10^{18}$ Hz, $e = 0.5$, and $g = 0$, corresponding to no acceleration. As in Paper I, we assume the jet to be of parabolic shape in the inner part ($x < 10^3$), with $\epsilon = 0.5$, and of conical shape with $\epsilon = 1$ in the external region ($x > 10^3$).

For the inner, parabolic zone, $\xi = 0.25$ and equation (13) gives $L_s(\nu) \propto \nu^{-(\alpha_0 + \xi/\eta)}$ for $\nu > \nu_b$, where ν_b is the maximum synchrotron frequency emitted by the largest region of the paraboloid. Since $\eta = 1$, the spectrum is steepened by $\Delta\alpha = 0.25$ above $\nu_b = \nu_{\max}(1)x_{\max}^{-\eta} \sim 10^{15}$ Hz.

In the conical zone $\xi = -0.5$, so that the inner regions dominate the emission down to their self-absorption frequency. From equation (13) we have $L_s(\nu) \propto \nu^{-(\alpha_0 + \xi/k_m)}$, which, for $m = 1$, $n = 2$, and $\epsilon = 1$ gives a flat spectrum of index zero, independent of the value of α_0. Thus the overall synchrotron spectrum is characterized by the three spectral indices: $\alpha_{\text{thick}} = 0$, $\alpha_0 = 0.5$, and $\alpha_1 = 0.75$, with the breaks at the self-absorption (ν_m) and maximum ($\nu_{\max}$) emitted frequency of the transition region of the jet, connecting the paraboloid and the cone. Variability time scales should, in this model decrease with increasing frequency, since only the smallest regions emit the highest frequencies.

For the inverse Compton emission we find $l = -0.25$ in the parabolic region, and $l = -1.5$ in the cone. Thus in both cases the IC flux derives mostly from the inner jet. In the range 1–10 keV it is characterized by the spectral index $\alpha_0 = 0.5$. The computed synchrotron and IC spectra are reported in Figure 1 and the relevant parameters are reported in Table 1.

Now let the plasma be accelerated according to equation (6) in the region where the jet shape is parabolic. This hypothesis is at least consistent with simple hydrodynamic models (Marscher 1980; Königl 1981). In this case the spectrum depends on the angle of view, and the integral in equation (13) cannot be expressed analytically. However analytic results can be obtained for $\nu > \nu_b$ in the limiting cases of $\theta \sim 0°$ or $\theta \sim 90°$, since $\delta(0°) \sim \Gamma$ and $\delta(90°) \sim 1/\Gamma$, for $\Gamma \gg 1$. Let us call $\lambda = g(2 + \alpha_0)$. If $\xi > \lambda$, for frequencies $\nu > \nu_b$, where ν_b is defined as before (but taking into account the Doppler correction), equation (13) yields the spectral indices

$$\alpha(\theta = 0°) = \alpha_0 + \frac{\xi + \lambda}{\eta}, \tag{14a}$$

$$\alpha(\theta = 90°) = \alpha_0 + \frac{\xi - \lambda}{\eta}, \tag{14b}$$

while, if $\xi \le \lambda$

$$\alpha(\theta = 90°) = \alpha_0 . \tag{14c}$$

Due to the dependence of the Doppler factor on R, the contribution of the outer regions is enhanced for observers at small angles and reduced for observers at large angles, while that of the innermost regions is unaffected. Correspondingly, the spectral indices in the range $\nu < \nu_b$ are respectively steeper (eq. [14a]) and flatter (eq. [14b]) than in the case of no acceleration.

TABLE 1

PARAMETERS OF THE MODELS SHOWN IN FIGURE 1[a]

Region	$1 < x < 10^3$	$10^3 < x < 10^6$
m	1	1
n	2	2
ϵ	0.5	1
η	1	2
g	0, 0.2	0
ξ[b]	0.25	−0.5
l[b]	−0.25	−1.5

[a] In Fig. 1 $B_0 = 10^3$ and $\tau_0 = 10^{-3}$ have been used.
[b] $\xi = 1 - \epsilon[n + m(1 + \alpha) - 2]$, $l = \xi - \epsilon(n - 1)$.

The full spectra numerically computed for $\lambda = 0.5$ are shown in Figure 1. At low frequencies the "flat" spectrum is maintained because outside the parabolic region the Doppler factor is assumed to be constant and the spectral shape is roughly independent from the viewing angle.

For the IC emission the effect is similar despite the fact that the intrinsic IC emission is stronger from the inner regions where beaming is weak. In fact, for small angles of view, the boosting effect reverses the dominance of the inner regions over the outer ones, since, in the parabolic region, $\lambda + l > 0$.

III. APPLICATION TO BLAZARS

For all blazars (33 objects) observed in the UV band with the *IUE* satellite before 1983 December a collection of data including radio, optical, UV, and X-ray flux densities, and infrared, optical and UV slopes was studied by Ghisellini *et al.* (1986). In an accompanying paper, Maraschi *et al.* (1986) considered all blazars (75 objects) observed in the X-ray band, 52 of which have known redshifts. Because of the large percentage of sources with known distance, the luminosity distribution in different bands could be studied. Both samples contain objects discovered by radio surveys (radio-selected objects) and a minority of sources that have been or could have been discovered from X-ray observations (X-ray–selected objects). The main conclusions drawn from these papers, for which we seek here an interpretation are the following:

1. Radio-selected blazars have steeper broad-band energy distributions than X-ray–selected ones. This statement holds also within the IR, optical, and ultraviolet ranges. This result is illustrated in Figure 2, where the average spectra of radio- and X-ray–selected objects are schematically reported.
2. Both classes have the same mean X-ray luminosity, but they differ by two orders of magnitude in the mean radio luminosities, the X-ray–selected ones being underluminous.
3. The "classical" radio-loud blazars may not be typical of the class of blazars as a whole, representing only a minority of sources in terms of absolute space density.

Our aim is to reproduce the average observed spectra reported in Figure 2 with a unique set of parameters and different angles of view. The simple parameter choice discussed for illustration purposes in the previous section is not adequate for this scope. Comparing Figures 1 and 2 we see an important discrepancy in the optical infrared range where the model spectra have the same spectral index while the observed ones are significantly different. Therefore the effects of acceleration must be present in the region of the jet emitting at optical and infrared frequencies. At the same time a significant steepening is observed, both for radio-selected and X-ray–selected objects, from the IR to the ultraviolet band.

In terms of our model the observed steepening requires that $\Delta\alpha^+ = (\xi + \lambda)/\eta$ as well as $\Delta\alpha^- = (\xi - \lambda)/\eta$ increase with decreasing size (increasing frequency). This cannot be obtained by increasing λ. The parameter η is constrained by the observed time scale at different frequencies. Imposing 1 hr ($R \sim 10^{14}$ cm) in the X-rays ($\nu = 10^{18}$ Hz) and 1 day ($R \sim 3 \times 10^{15}$ cm) in the ultraviolet ($\nu = 10^{15}$ Hz), one deduces that the value of η must be near to 2, at least for $1 < x < 50$. For larger values of x, η should be smaller, otherwise the maximum frequency rapidly approaches the self-absorption frequency and the emission is quenched. Therefore a larger $\Delta\alpha$ cannot result from a decrease of η with increasing frequency. The only viable choice is then to increase ξ, i.e., to split the inner region in two parts with larger ξ in the innermost one.

The results of models of this type are shown in Figure 3 where for simplicity we do not include the outer region ($x > 10^3$) responsible for the radio emission. The relevant parameters for these models are reported in Table 2. Assuming that the bulk Lorentz factor Γ increases steadily with distance (for $1 < x < 10^3$) one obtains the synchrotron spectra shown in Figure 3*a*. Comparing these with the observational results reported in Figure 2 one sees that the infrared to X-ray energy distributions are reasonably well reproduced. The observed monochromatic luminosities fall in between the curves for aspect angles of 20° and 60°. In order not to produce excessive

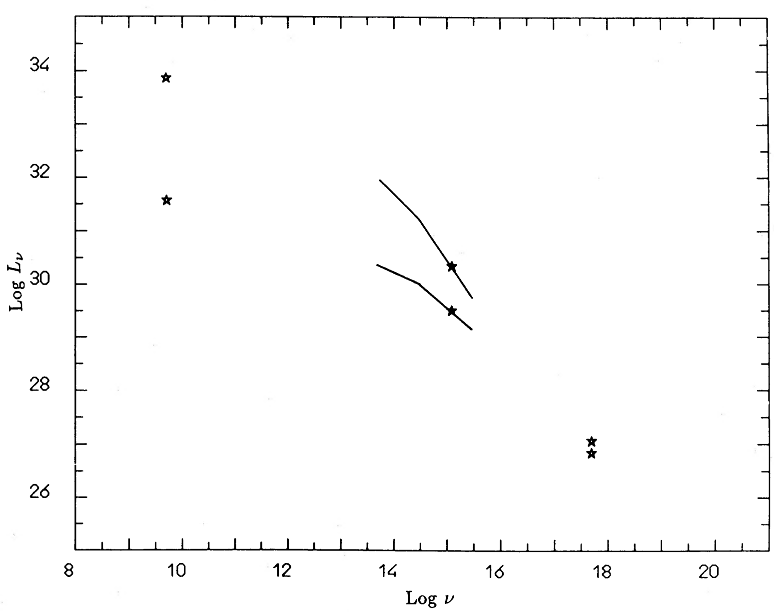

FIG. 2.—The average monochromatic luminosities and spectral slopes of a sample of blazars as derived by Ghisellini *et al.* (1986) and Maraschi *et al.* (1986) are shown separately for radio-selected (*upper points*) and X-ray–selected objects (*lower points*).

TABLE 2

PARAMETERS OF THE MODELS REPORTED IN FIGURE 3

Region	$1 < x < 50$	$50 < x < 10^3$
m	0.5	1
n	1.25	2
ϵ	0.5	0.5
η	1.5	2
g	0.2	0.2
ξ[a]	1	0.25
l[a]	0.88	−0.25
m	0.5	1
n	1.25	2
ϵ	0.5	0.5
η	1.5	2
g	0	0.3
ξ[a]	1	0.25
l[a]	0.88	−0.25
m	1	1.5
n	0.5	1.25
ϵ	0.5	0.5
η	1.5	2
g	0.2	0.2
ξ[a]	1	0.25
l[a]	1.25	0.13

NOTE.—The first set of parameters refers to Figures 3*a* and 3*c*, the second to Fig. 3*b*, and the third to Fig. 3*d*. For all models $B_0 = 10^3$ and $\tau_0 = 10^{-3}$ have been used.

[a] $\xi = 1 - \epsilon[n + m(1 + \alpha) - 2]$, $l = \xi - \epsilon(n - 1)$.

anisotropy the acceleration must be very slow ($g = 0.2$).

We have also considered the possibility that the innermost X-ray–emitting region is associated with the isotropic core and acceleration starts at somewhat larger distances, in between the X-ray and ultraviolet emitting regions. The result is illustrated in Figure 3*b*, where, with all the other parameters fixed as in Figure 3*a*, acceleration has been introduced only for $50 < x < 10^3$, but with a larger value of g ($g = 0.3$).

It is useful to illustrate here also the role of the other important parameters. The ξ parameter results from a combination of the exponents n, m, and ϵ, describing, respectively, the radial dependence of the relativistic particle density, the magnetic field, and the cross-sectional radius of the jet (see § II). For the shape of the convoluted synchrotron emission the value of ξ is more important than the separate values of n, m, and ϵ. However, m and n determine the magnetic field and particle density and therefore the synchrotron self-absorption frequency. Therefore some dependence on the values of these parameters is also present.

Especially sensitive to the magnetic field behavior is the self-Compton emission: this is determined by the initial values of the magnetic field and particle density and also by the radial dependences given by n and m. If B decreases too rapidly (large m) the self-Compton emission contribution becomes excessive.

The IC spectra for the model reported in Figure 3*a* are shown in Figure 3*c*. Figure 3*d* shows the results of a model which differs from that of Figure 3*c* only in the radial decay of the magnetic field and particle density which are chosen in both cases so as to give the same value of ξ. In fact, the synchrotron spectra of the two models are indistinguishable, but the one in which the field decays more rapidly yields an IC contribution largely in excess of the observational limits.

In discussing the agreement of computed models with the average spectra reported in Figure 2 one should know to what average aspect angles the two samples of radio-selected and X-ray–selected objects correspond. For a complete sample the angle could be computed given a model for the anisotropy. However, the samples from which the average spectra were derived, although objectively chosen, are not complete. Note that, even if the X-ray emission were isotropic, which would imply that pure X-ray selection is unbiased with respect to angle, the procedure of optical identification adopted in most cases requires a radio flux, although weak, and an optical continuum from the nucleus of the galaxy. Thus the identification procedure introduces a bias in favor of smaller angles, which is not easily quantifiable. In view of these uncertainties we will simply assume that for X-ray–selected objects the average aspect angle is between 90° and 60° while for the radio-selected ones it is between 20° and 0°.

The models selected to account for the observed average spectra are presented in Figure 4. As argued above, the successful models must include at least three regions, whose boundaries we keep fixed: $1 < x < 50$ (region 1), $50 < x < 10^3$ (region 2), $10^3 < x < 3 \times 10^6$ (region 3). The minimum size R_0 is also fixed at 10^{14} cm by the constraint that the minimum variability time scale in the X-ray band is 1*h*. All the physical quantities vary continuously throughout the jet. Only the gradients are discontinuous at the boundaries of the regions.

Figures 4*a* and 4*b* show the synchrotron and inverse Compton spectra for the case in which acceleration is assumed to occur continuously in regions 1 and 2. The relevant parameters are reported in Table 3. They differ for the different values of m and n, chosen to let the IC flux come from the intermediate region in the model of Figure 4*a*, and from the most extended zone for the model of Figure 4*b*.

Figure 4*c* shows the results for the case in which acceleration is present only in region 2. The main difference between the two classes of models is in the as yet unobserved spectral region between the far ultraviolet and soft X-rays. In this range the second class of models yields a flattening of the synchrotron spectrum for small aspect angles, which is impossible in the first one. As shown in Figure 2, a flattening is suggested by the comparison of the X-ray flux with the extrapolation of the UV spectrum for the radio-selected BL Lac objects which are supposedly observed at small angles. Alternatively a flattening in the EUV-soft X-ray region could be attributed to a Compton contribution which is present in both classes of models. However, if the flat spectrum is due to the inverse Compton process, it is expected to extend up to the hard X-rays.

A general feature of the selected models is that, while the synchrotron emission in the X-ray band derives from the most compact region of the jet and is therefore quasi-isotropic, the X-rays produced through the IC process originate predominantly in the outer regions and are therefore beamed. Thus for small sight angles the IC X-rays may be important, while for large sight angles synchrotron X-rays contribute predominantly to the observed flux.

IV. DISCUSSION

The proposed model can account for the difference in spectral shapes of radio-selected and X-ray–selected blazars. It may seem that this is done in terms of a large number of parameters. On the other hand each homogeneous SSC model must specify the volume, the density and energy distribution of electrons

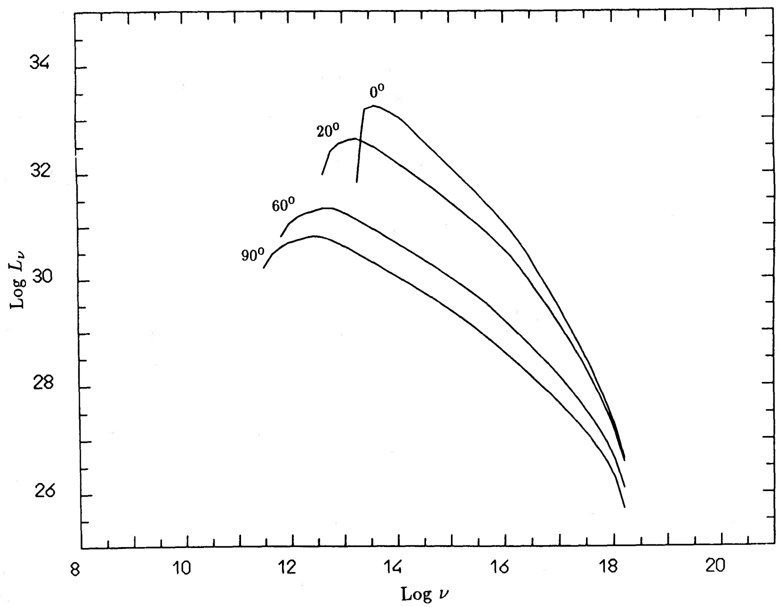

FIG. 3a

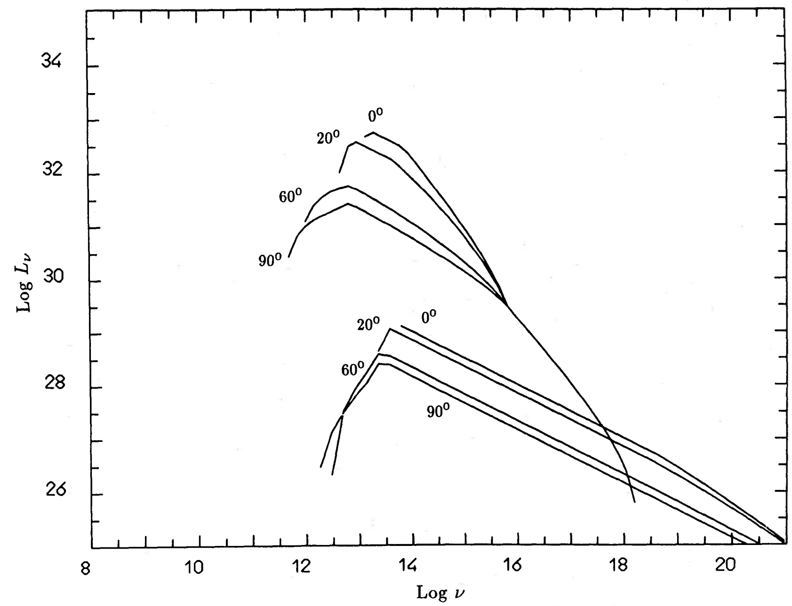

FIG. 3b

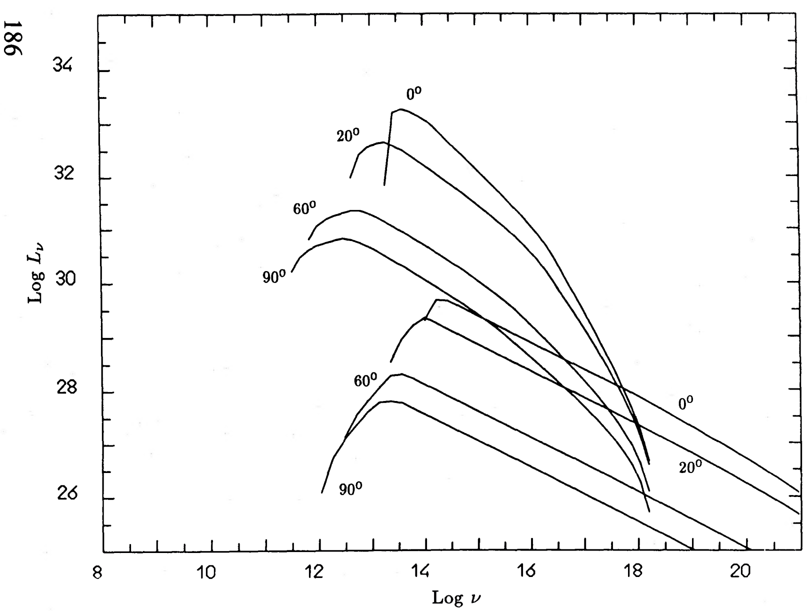

FIG. 3c

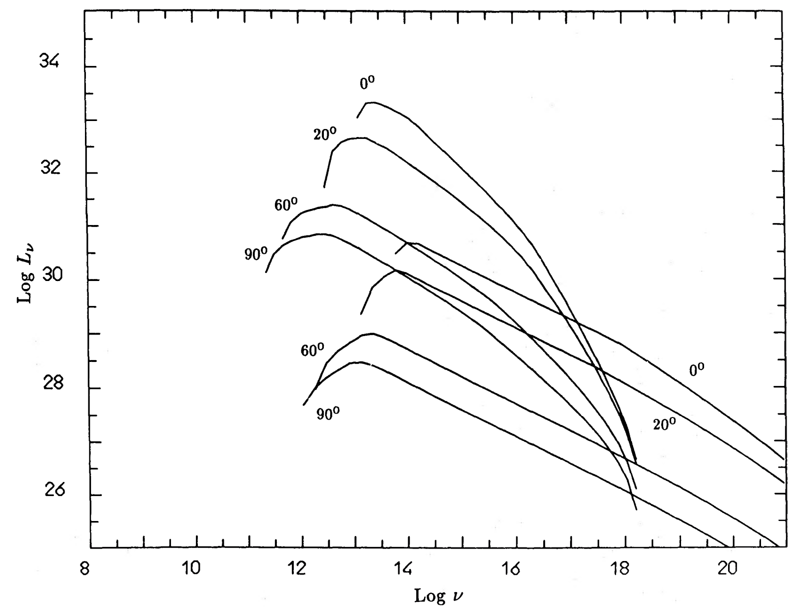

FIG. 3d

FIG. 3.—(*a*) Synchrotron emission spectra from the inner part ($x < 10^3$) of a relativistic jet described by the parameters reported in Table 2 observed at different viewing angles. Bulk acceleration occurs continuously throughout $1 < x < 10^3$ with $g = 0.2$. (*b*) Same as (*a*) but with bulk acceleration occurring only for $50 < x < 10^3$ with $g = 0.3$. (*c*) Same as (*a*) with addition of inverse Compton emission spectra. (*d*) Same as (*c*) but with different values of *m* and *n* (see Table 2).

TABLE 3

PARAMETERS OF THE MODELS REPORTED IN FIGURE 4

Region	$1 < x < 50$	$50 < x < 10^3$	$10^3 < x < 3 \times 10^6$
m	0.5	1	1
n	1.25	1.5	1.5
ϵ	0.5	1	1
η	1.8	1.2	1.2
g	0.15	0.15	0
ξ[a]	1	0	0
l[a]	0.88	−0.5	−0.5
m	0.5	1.5	1.5
n	1.25	0.75	0.75
ϵ	0.5	1	1
η	1.8	1.2	1.2
g	0.15	0.15	0
ξ[a]	1	0	0
l[a]	0.88	0.25	0.25
m	0.5	1	1
n	1.25	2	1.5
ϵ	0.5	0.5	1
η	1.5	2	1
g	0	0.3	0
ξ[a]	1	0.25	0
l[a]	0.88	−0.25	−0.5

NOTE.—The first set of parameters refers to Fig. 4*a* (for which $B_0 = 700$ and $\tau_0 = 5 \times 10^{-4}$), the second to Fig. 4*b* ($B_0 = 5 \times 10^3$ and $\tau_0 = 2.5 \times 10^{-5}$), and the third to Fig. 4*c* ($B_0 = 10^3$ and $\tau_0 = 3 \times 10^{-4}$).

[a] $\xi = 1 - \epsilon[n + m(1 + \alpha) - 2]$, $l = \xi - \epsilon(n - 1)$.

and the magnetic field. Here we have three regions in which these physical quantities vary according to power laws. Thus the model is equivalent to three discrete SSC components which can be joined monotonically.

A description in terms of a number of components which may be associated with shocks in the flow may be closer to reality in specific objects. However, the regularity of the observed spectra demands well defined relations between the components. Our continuous description should then be relevant.

The requirement that the observed differences between the overall spectra of X-ray–selected and radio-selected BL Lac objects is solely due to orientation effects imposes stringent conditions on the properties of relativistic jets. We require a first region in which the rest frame synchrotron power per unit frequency $P_s(\nu)$ increases with increasing distance along the jet, followed by two regions in which $P_s(\nu)$ is nearly constant and eventually decreases with increasing distance.

The main bulk accleration occurs throughout the first and second or possibly only in the second region, reaching bulk Lorentz factors $\Gamma \simeq 3$–5. If the smallest dimension is 1 light hour, the magnetic field must be of the order of 300–1000 G and slowly decreasing with radius. The density of relativistic electrons at the core is 10^7–10^8 cm^{-3} with maximum energy for the individual electrons of $\sim 10^4$ MeV. The lifetime of such electrons is much shorter than the crossing time, so that they must be replenished continuously by an acceleration mechanism, as first emphasized by Blandford and Rees (1978). Thus one cannot think of the flow as adiabatic, which constitutes, *a posteriori*, a justification for our empirical approach.

The ratio U_B/U_e of the magnetic energy density to relativistic electron energy density is much greater than unity for the inner part of the jet for all the models of Figure 4. This dominance of the magnetic field is maintained throughout the entire jet for the models in Figure 4*a* and 4*c*, while the model in Figure 4*b* in which we force a large Compton contribution from the extended component results to be particle dominated in this region. The general dominance of the magnetic energy density is at least in agreement with the observed degree of polarization. The relativistic electrons in the inner part of the jet have roughly the same energy of protons at their virial temperature. Then proton densities of the same order of the relativistic electron density in the jet give the same pressure.

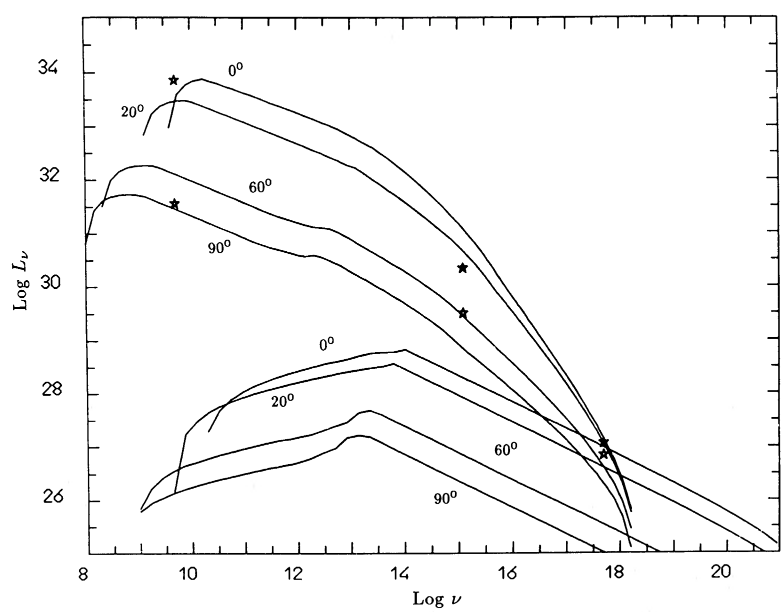

FIG. 4*a*

FIG. 4.—Synchrotron and Inverse Compton spectra from a relativistic jet observed at different angles for the model parameters reported in Table 3. Stars represent the observed average monochromatic luminosities of radio-selected (*upper*) and X-ray–selected (*lower*) Blazars (see Fig. 2). (*b*) differs from (*a*) mainly in the Inverse Compton emission. (*c*) Refers to a case in which bulk acceleration occurs within $50 < x < 10^3$. In all cases $x = R/R_0$ with $R_0 = 10^{14}$ cm.

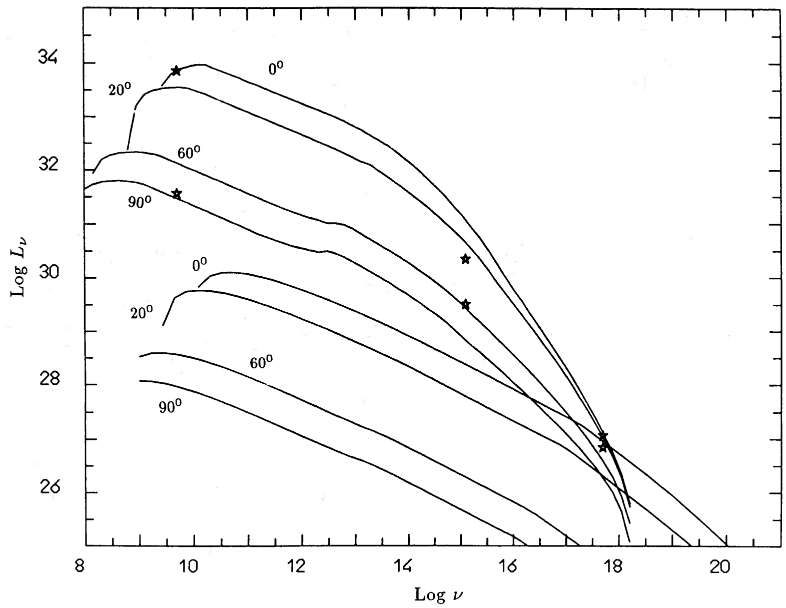

FIG. 4b

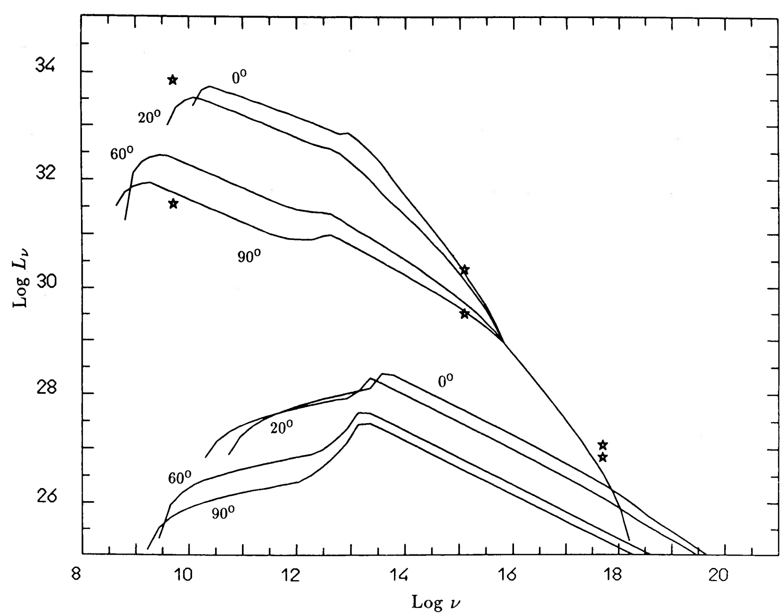

FIG. 4c

This proton density corresponds to an accretion rate of $\sim 10^{22}$ g s^{-1}, orders of magnitude smaller than the critical one. Thus a modest accretion flow, if at the virial temperature, would be sufficient to confine the inner part of the jet.

The adopted intrinsic particle distribution ($p = 2 \rightarrow \alpha_0 = 0.5$) is consistent with the hypothesis of continuous injection of monoenergetic particles in the absence of electron-positron pair production. We do not expect pair effects to be very important for the physical parameters discussed above. In fact the total luminosity to size ratio is only marginally above the threshold for pair production in the innermost region and the fraction of the total luminosity emitted above 1 MeV through the Compton process in the inner region is $\sim 50\%$, since the magnetic and radiation energy densities are nearly equal. Furthermore, pairs mainly contribute to the synchrotron emission at low energies, where self-absorption is important (see, e.g., Ghisellini 1987, 1988).

The model was constructed so as to explain the two average broad-band energy distributions. This implies that the luminosity profile has a maximum in the intermediate part of the jet, at a distance corresponding to $x \sim 50$–100. In so doing we were forced to assume that, in the X-ray band, where the luminosities cluster around a single average value, the maximum synchrotron frequency is reached. This condition determines the steepening which appears at the high-energy end of the synchrotron spectra. Thus the model predicts that spectra within the X-ray range will be generally steep. Only in sources where the Compton contribution is important, X-ray spectra may be flatter, therefore the shape of the X-ray spectrum will be a signature of the dominant emission process. We note that in the sample of objects bright enough to be observable with the medium energy experiment of the EXOSAT satellite the X-ray spectra turn out to be rather steep, with an average energy spectral index of 1.5 (Maraschi and Maccagni 1988).

A general feature of the model is that in the X-ray range the importance of the Compton contribution depends on the angle. Compton radiation from the inner regions can be comparable to the synchrotron emission. However, Compton radiation from the outer regions which are affected by Doppler boosting will be larger for sources seen head on and smaller for sources seen at large angles. Correspondingly the short time-scale variability which may be associated with the inner regions will be observable in sources seen from the side but masked by the contributions from beamed outer regions in objects seen at small angles.

This can explain the peculiar behavior of some BL Lac objects, such as 0735+178 (Bregman *et al.* 1984), which shows faster variability in the UV band than in X-rays. If the proposed model is correct, the IC flux coming from the intermediate regions of the jet can give a sizable contribution to the X-ray band only for sources beamed at us (radio-selected), which, on average, are then predicted to show less rapid X-ray variability than X-ray–selected sources. The opposite will be true at low frequencies, where objects beamed at us are expected to exhibit larger and faster variability than unbeamed (X-ray–selected) ones.

Since the maximum bulk Lorentz factors derived in this model are small, $\Gamma \simeq 3$–5, for a given X-ray luminosity the number ratio of radio strong to radio weak objects is expected to be 20–100. This implies that, when the sample of X-ray–selected objects will be large enough, some radio strong objects should be found to belong to this group.

In summary, the apparent simplicity of BL Lac spectra is interpreted as being due to the convoluted emission from a relativistic jet whose innermost regions at rest emit the highest frequencies, while outer regions, with increasing bulk velocity, emit lower frequencies. The observed broad-band energy distributions strongly constrain the properties of such jets. The model predicts that rapid X-ray variability is associated with steep X-ray spectra, while objects with flat X-ray spectra are expected to be more variable at optical to radio frequencies. The absolute space density of radio strong objects ($\alpha_{ro} > 0.5$) should be $(1–5) \times 10^{-2}$ of that of radio weak objects with the same X-ray luminosity.

REFERENCES

Blandford, R. D. 1987, in *Superluminal Radio Sources*, ed. J. A. Zensus and T. J. Pearson (Cambridge: Cambridge University Press), p. 310.
Blandford, R. D., and Rees, M. J. 1978, *Pittsburgh Conf. in BL Lac Objects*, ed. A. N. Wolfe (Pittsburgh: University of Pittsburgh Press), p. 328.
Blumenthal, G. R., and Gould, R. J. 1970, *Rev. Mod. Phys.*, **42**, 237.
Bregman, J. N., *et al.* 1986, *Ap. J.*, **276**, 454.
Browne, I. W. A., and Murphy, D. W. 1987, *M.N.R.A.S.*, **226**, 601.
Ghisellini, G. 1987, *M.N.R.A.S.*, **224**, 1.
———. 1988, *M.N.R.A.S.*, submitted.
Ghisellini, G., Maraschi, L., Tanzi, E. G., and Treves, A. 1986, *Ap. J.*, **310**, 317.
Ghisellini, G., Maraschi, L., and Treves, A. 1985, *Astr. Ap.*, **146**, 204 (Paper I).
Kardashev, N. S. 1962, *Soviet Astr.—A.J.*, **6**, 317.
Königl, A. P. 1981, *Ap. J.*, **243**, 700.
Impey, C. D., and Neugebauer, G. 1988, *A.J.*, **95**, 307.
Maraschi, L. 1987, *Variability of Galactic and Extragalactic X-Ray Sources*, ed. A. Treves (Milano: Assn. Adv. Astr.), p. 101.
Maraschi, L., Ghisellini, G., Tanzi, E. G., and Treves, A. 1986, *Ap. J.*, **310**, 325.
Maraschi, L., and Maccagni, D. 1988, in *X-Ray Astronomy with EXOSAT*, ed. N. White and R. Pallavicini, *Mem. Soc. Astr. Italiana.*, Vol. **59**, in press.
Marscher, A. P. 1980, *Ap. J.*, **235**, 386.
Reynolds, S. P. 1982, *Ap. J.*, **256**, 13.
Stocke, J. T., Liebert, J., Schmidt, G. D., Gioia, I. M., Maccacaro, T., Schild, R. E., Maccagni, D., and Arp, H. C. 1985, *Ap. J.*, **298**, 619.

GABRIELE GHISELLINI: Institute of Astronomy, Madingley Road, Cambridge CB3 0HA, England, UK

LAURI MARASCHI: Dipartimento di Fisica, Sezione di Astrofisica, Universita' di Milano, Via Celoria 16, 20133 Milano, Italy